LOW REYNOLDS NUMBER CONVECTIVE HEAT TRANSFER ACROSS A CIRCULAR CYLINDER WITH UNIFORM VOLUMETRIC ENERGY DISSIPATION

M. S. Kamran, H. Ali, F. Noor, S. Imran, A. Hussain and H. S. Wang*

Faculty of Mechanical Engineering, University of Engineering and Technology, Lahore, Pakistan
*School of Engineering and Materials Science, Queen Mary University of London, Mile End Road, London E1 4NS, UK
Corresponding author email: m.s.kamran@uet.edu.pk

ABSTRACT: Flow and heat transfer across a circular cylinder with uniform volumetric energy dissipation under unconfined condition was numerically investigated using Ansys Fluent 12.0. The fluid was water with Prandtl number 7. The Reynolds number varied from 10 to 40. The results were compared with constant surface temperature and constant heat flux at the surface of the cylinder. It was found that the average Nusselt numbers with uniform energy dissipation (UED) in the cylinder were about 11% lower than those with constant heat flux (CHF) boundary condition and approximately 4% higher than those with constant surface temperature (CST) boundary condition. The average Nusselt numbers under different boundary conditions were also correlated with the Reynolds numbers.

Key words: convective heat transfer, cylinder, uniform volumetric energy dissipation, numerical simulation

(Received 7-8-14 Accepted 06-03-15)

INTRODUCTION

The demand for energy has led to a large global effort to develop and improve existing technologies and to find new ones. Magnetic refrigeration and heating are environmentally friendly emerging technologies with a realistic potential to replace the conventional vapour-compression refrigeration (Yu *et al*., 2010). Recently, various reviews (Gschneidner and Pecharsky, 2008; Kitanovski and Egolf, 2010; Yu *et al*., 2010) reveal that in all up-to-date prototypes reported, the pressure drop of the fluid in the regeneratoris significantly high and heat transfer rate is relatively low. This limits the performance of the refrigerators and heat pumps and has become a major obstacle.

Flow and heat transfer over circular cylinders are very common in many applications and have been extensively studied experimentally and numerically (Eckert and Soehngen, 1953; Zukauskas *et al*., 1985; Williamson, 1996; Hanafi *et al.*, 2002; Nakamura and Igarashi, 2004; Yoon *et al*., 2007; Henderson, 1995; Bharti *et al*., 2007 and Park *et al*., 1998).The convective heat transfer over an array of cylinders under conjugate boundary condition, i.e., uniform internal heating within each cylinder has been numerically studied for the Reynolds number(*Re*)ranging from 100 to 400 and *Pr* is 0.71(Wang and Georgidias, 1996).

For active magnetic regenerator, usually a very low mass flow rate of the working fluid yields optimal performance. The Reynolds number of the fluid flow in the prototypes reported so far is generally less than 50 (Nielson *et al*., 2009). During the magnetization and demagnetization processes under a magnetic field of the magnetic refrigeration cycle, the energy dissipation occurs in the form of heat source and sink(conjugate boundary condition).Thus, cylinders made of the magnetocaloric material (MCM) can be a possible alternative in the regenerative heat exchanger. In this study, the flow and heat transfer over a single circular cylinder with uniform and constant volumetric energy dissipation is numerically investigated. The literature survey reveals that the flow and heat transfer characteristics for very low Re (below 100) have not been investigated. Thus, the present simulation is performed for low Reynolds number range. The present work investigates the influence of various boundary conditions for circular cylinder made of magnetocaloric material.

MATERIALS AND METHOD

Physical model and coordinate: The schematic diagram of the physical model and coordinate have been illustrated in figure (1). A circular cylinder of diameter d was placed in an unconfined fluid flow field having free stream velocity U_∞ and temperature T. The fluid was water. To simplify, the following assumptions were made: (1) volumetric energy dissipation rate $\dot{q}$within the cylinder was taken to be uniform and constant; (2) the flow was laminar; (3) the flow was two dimensional (2D), incompressible and steady and (4) the properties of the cylinder and the fluid were constant. The Cartesian coordinate (x, y) was taken from the centre of the cylinder. The angle θ was measured from the front stagnation point.

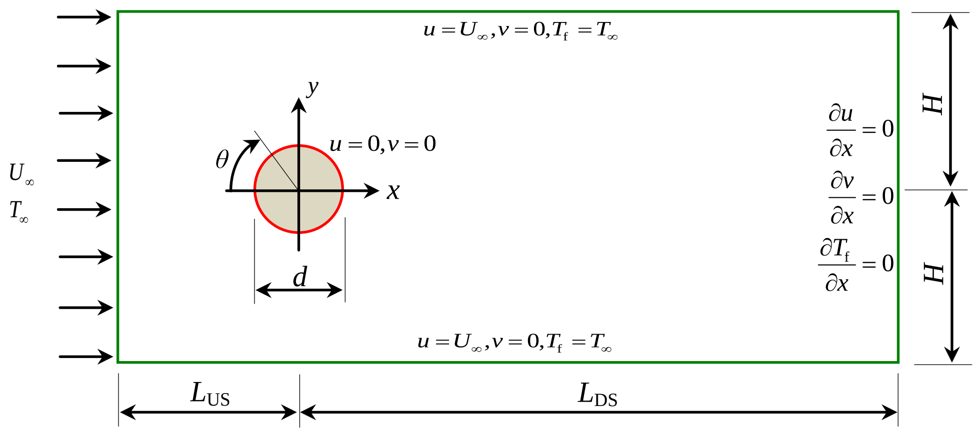

Fig-1:Showing schematic diagram of the physical model and coordinate

Governing equations:For two-dimensional, incompressible, steady, laminar flow with constant properties, the governing equations for the fluid region are as follows (Versteeg and Malalasekera, 2007)

Mass conservation

$$\frac{\partial u}{\partial x} + \frac{\partial v}{\partial y} = 0 \quad (1)$$

Momentum conservation

$$u\frac{\partial u}{\partial x} + v\frac{\partial u}{\partial y} = -\frac{1}{\rho}\frac{\partial p}{\partial x} + \nu\left(\frac{\partial^2 u}{\partial x^2} + \frac{\partial^2 u}{\partial y^2}\right) \quad (2)$$

$$u\frac{\partial v}{\partial x} + v\frac{\partial v}{\partial y} = -\frac{1}{\rho}\frac{\partial p}{\partial y} + \nu\left(\frac{\partial^2 v}{\partial x^2} + \frac{\partial^2 v}{\partial y^2}\right) \quad (3)$$

Energy conservation

$$u\frac{\partial T}{\partial x} + v\frac{\partial T}{\partial y} = \alpha\left(\frac{\partial^2 T}{\partial x^2} + \frac{\partial^2 T}{\partial y^2}\right) \quad (4)$$

The energy conservation within the solid cylinder is as follows

$$\alpha\left(\frac{\partial^2 T}{\partial x^2} + \frac{\partial^2 T}{\partial y^2}\right) + \frac{\dot{q}}{\rho C_p} = 0 \quad (5)$$

Computational domain and its boundary conditions: The computational domain, as shown infigure(1), was determined by the height *H*, upstream length L_{US} and downstream length L_{DS}. The domain was discretised into quadrilateral cells (Fig 2). The mesh density was high for the regions of large gradients of velocity and temperature and mesh density was kept low where the gradients were small (Versteeg and Malalasekera, 2007).

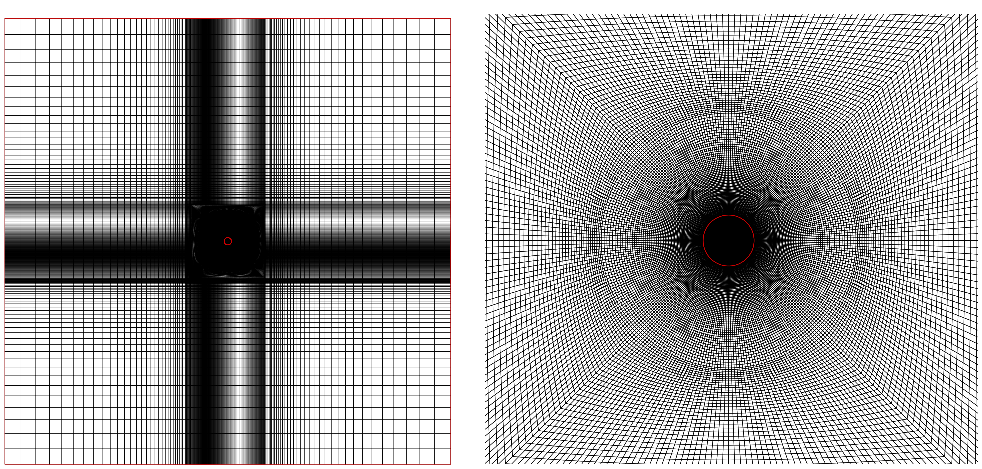

(a) (b)

Fig-2: Showing computational domain discretisation (a) entire domain (b) detailed view closer to the cylinder

The boundary conditions are as below:

$$u = U_\infty,\ v = 0, T = T_\infty \quad \text{at} \quad x = -L_{US} \quad (6)$$

$$\frac{\partial u}{\partial x} = 0,\ \frac{\partial v}{\partial x} = 0,\ \frac{\partial T}{\partial x} = 0 \quad \text{at} \quad x = -L_{DS} \quad (7)$$

$$u = 0, v = 0 \quad \text{at} \quad x^2 + y^2 - 0.25d^2 = 0 \qquad (8)$$

$$u = U_\infty, v = 0, T = T_\infty \quad \text{at} \quad y = \pm H \qquad (9)$$

Data reduction: The drag coefficient C_D is defined by (Batchelor, 2000), as

$$C_D = F_D / (0.5 A_f U_\infty^2) \qquad (10)$$

The local Nusselt number

$$Nu_\theta = \left.\frac{\partial T^*}{\partial n}\right|_{\text{wall}} \quad \text{for CST} \qquad (11a)$$

$$Nu_\theta = h_\theta d / \lambda \quad \text{for CHF and UED} \qquad (11b)$$

Where T^* is the dimensionless temperature defined as $T^* = (T - T_\infty)/(T_w - T_\infty)$, n is normal to the surface of cylinder and h_θ is the local heat-transfer coefficient

$$h_\theta = q_\theta / (T_w - T_\infty) \qquad (12)$$

The surface average Nusselt number was calculated by

$$Nu_{av} = \frac{1}{2\pi} \int_0^{2\pi} Nu_\theta d\theta \qquad (13)$$

Numerical method: The finite volume method was adopted to discretise the governing equations. The semi implicit method for pressure linked equations (SIMPLE) algorithm was used for solving the pressure and velocity fields and the second order upwind difference scheme was used to discretise the convective terms in momentum and energy equations. The numerical simulation was carried out using the commercial software Ansys Fluent. The properties were taken at a reference temperature i.e. 20 ^{o}C. The *Pr* number of water was constant of 7 and the *Re*number varied from 10 to 40.For comparison, the calculation for the cases of constant surface temperature and constant heat flux boundary conditions were also performed (Tab 1).

Grid and domain size independence*:* The effect of domain size was examined by evaluating the drag coefficient C_D and average Nusselt number Nu_{av} for different upstream length L_{US}, downstream length L_{DS} and height *H*(tab. 1). The numerical conditions are given in Table-1. A domain size with H/d, L_{US}/d and L_{DS}/d of 30, 30 and 30, respectively, was chosen.

The mesh size was determined by evaluating the values of C_D and Nu_{av} for different number of grid (Tabs 2-3). For the cases of CST and CHF boundary conditions a mesh size with grid number of 29,600 was chosen. For the case of UED, a mesh size with grid number of 33,050 was chosen.

Table-1:Showing effect of domain size on C_D and Nu_{av}at *Re* = 40 and *Pr* = 7 for CST, CHF and UED

H/d	L_{US}/d	L_{DS}/d	C_D	Nu_{av}		
				CST	CHF	UED
10	10	40	1.617	7.279	8.512	7.617
10	15	40	1.602	7.255	8.433	7.598
10	15	50	1.602	7.257	8.505	7.595
20	10	20	1.588	7246	8.487	7.568
20	10	40	1.589	7.247	8.488	7.571
20	15	20	1.557	7.200	8.452	7.554
20	15	40	1.557	7.201	8.454	7.557
20	20	20	1.545	7.182	8.419	7.517
20	20	40	1.545	7.184	8.420	7.519
30	10	20	1.587	7.245	8.376	7.582
30	10	40	1.587	7.245	8.375	7.582
30	15	20	1.538	7.196	8.433	7.943
30	15	40	1.553	7.196	8.433	7.943
30	20	20	1.538	7.175	8.393	7.507
30	20	40	1.538	7.175	8.395	7.507
30	30	20	1.526	7.158	8.387	7.487
30	30	30	1.527	7.157	8.388	7.488
40	40	40	1.518	7.145	8.374	7.475
50	50	50	1.518	7.138	8.366	7.468

Table-2:Showing effect of mesh size on C_D and Nu_{av} under CST and CHF conditions at *Re* = 40 and *Pr* = 7

No. of cells	C_D	Nu_{av}	
		CST	CHF
19,200	1.533	8.410	7.182
29,600	1.528	8.392	7.162
40,000	1.527	8.389	7.158
58,800	1.527	8.388	7.158

Table-3: Effect of mesh size on C_D and Nu_{av}under UED conditions at *Re* = 40 and*Pr* = 7

No. of cells	C_D	Nu_{av}
		UED
20,504	1.528	8.410
33,050	1.528	8.392
46,728	1.528	8.389
69,027	1.528	8.388

RESULTS AND DISCUSSION

To validate present numerical results, the local Nusselt number and the drag coefficient were compared with the earlier numerical results by (Bharti, *et al*., 2007) and experimental data by (Eckert *et al*., 1953). The local Nusselt number Nu_θ along with the surface of the cylinder for both CST (a) and CHF (b) boundary conditions have been presented in figure (3). It was found that the results of the present study were in agreement with those of (Bharti *et al*., 2007). The numerical results agreed well with the experimental data in the region of θ less than about 80^o and lower than the experimental data in the region of θ great than about 80^o. The discrepancy may be due to the conditions between the measurements and numerical simulations. Comparison of drag coefficients between the present study and earlier results of (Park *et al*., 1998 and Henderson 1995) have been presented in Table 4.

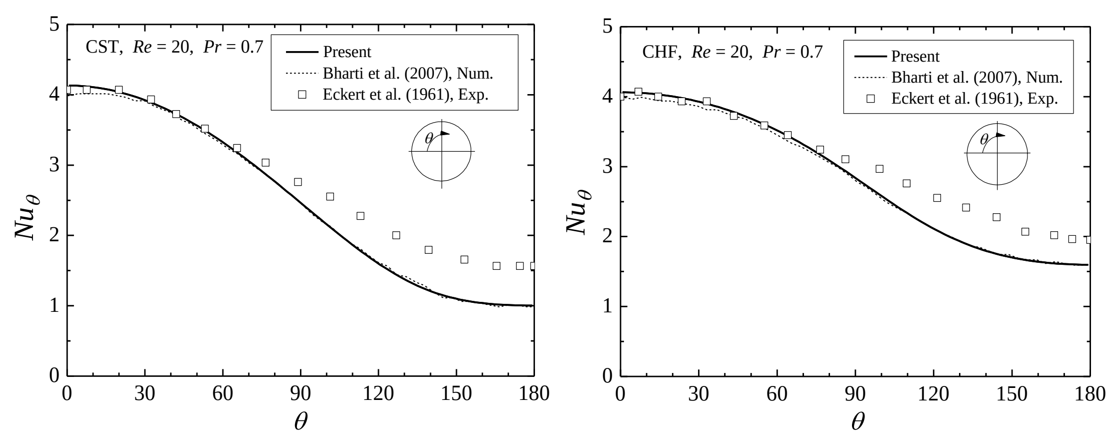

(a) (b)

Fig-3: Comparison of Nu_θ(a) constant surface temperature (b) constant heat flux

Table-4: Comparison of drag coefficients at different *Re*

Re	C_D		
	Park et al. (1998)	Henderson (1995)	Present study
10	2.78	-	2.836
20	2.01	-	2.046
30	-	1.73	1.721
40	1.51	1.54	1.526

The flow field as shown in figure (4).Two steady, symmetric vortices were found behind the cylinder and the wake region increased as the *Re*number increased. The dimensionless temperature field across the cylinder for the condition of UED at four *Re*numbers for the diameter of 10.0, 5.0 and 1.0 mm, respectively as has been presented in figures (5-7)

It can be seen that when the diameter of the cylinder was reduced, the temperature field in the wake region decreased.

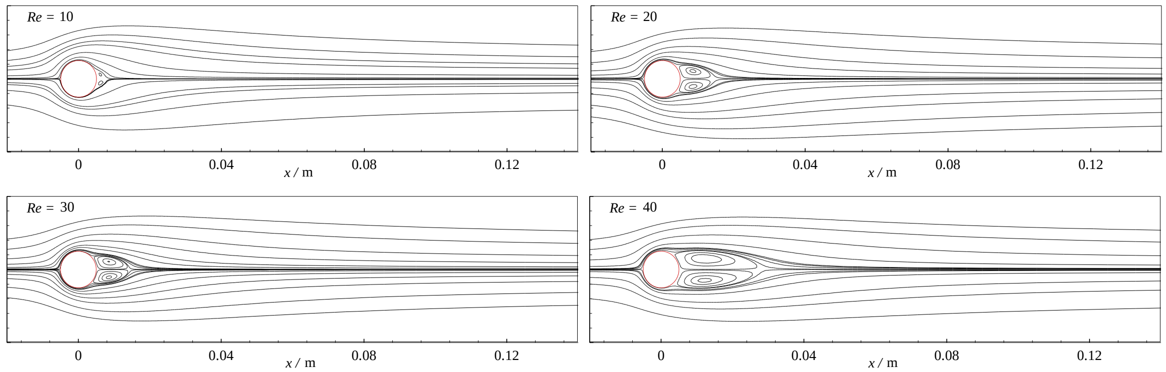

Fig-4: Showing flow streamlines for different *Re*. *Pr* = 7.

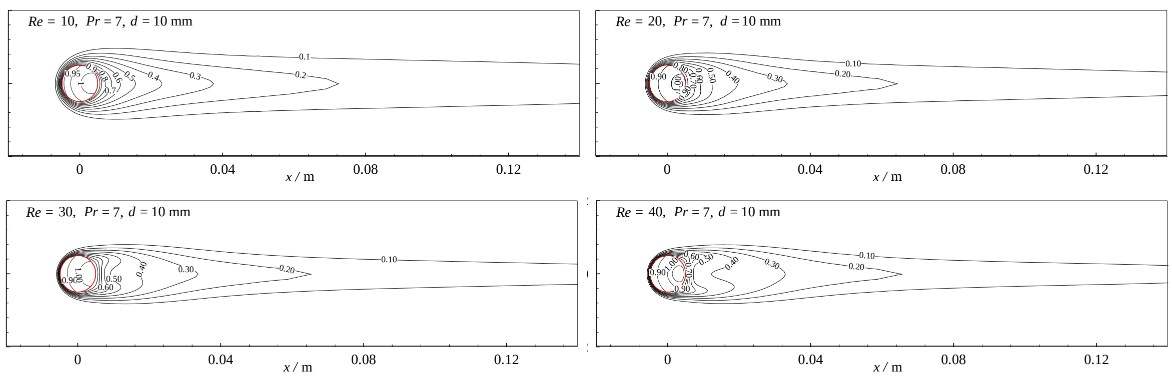

Fig-5:Showing dimensionless temperature field $T^{*}=(T-T_{\infty})/(T_{\max}-T_{\infty})$ **across the cylinder with UED (d = 10 mm)**

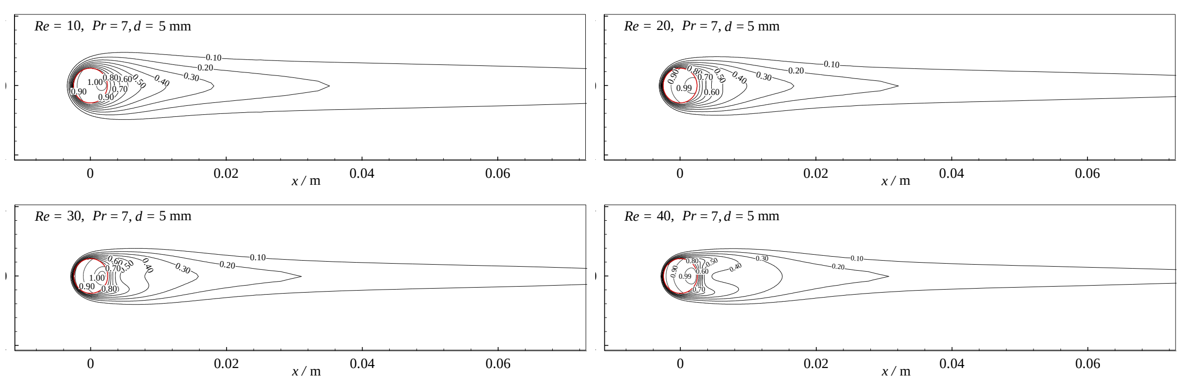

Fig- 6:Showing dimensionless temperature field $T^{*}=(T-T_{\infty})/(T_{\max}-T_{\infty})$ **across the cylinder with UED (d = 5 mm)**

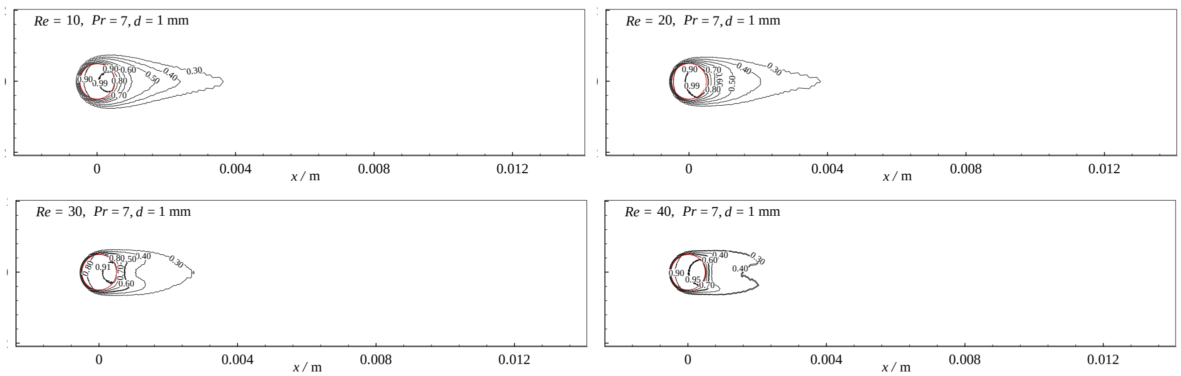

Fig-7:Showing dimensionless temperature field $T^* = (T - T_\infty)/(T_{\max} - T_\infty)$ **across the cylinder with UED (d = 1 mm)**

Local Nusselt number Nu_θalong the cylinder surface was obtained using Eq. (11) and has been shown in figure (8)for three boundary conditions and four Reynolds numbers. This was observed that Nu_θ was a function of the angular position θ along the cylinder, *Re* and the thermal boundary conditions. The Nu_θ look the maximum value at front stagnation point and decreased till the separation point. The Nu_θ increased again in the rear stagnation region due to flow circulation and reattachment but the value was considerably lower than that at the front stagnation point. The Nu_θ also increased with increasing *Re*. The values of Nu_θ were the highest for UED condition and slightly higher for UED than CST condition. Local Nusselt number was found to be independent of the cylinder size. Similar results have been reported by (Zukauskas *et al*., 1985 and Bharti *et al.*, 2007).

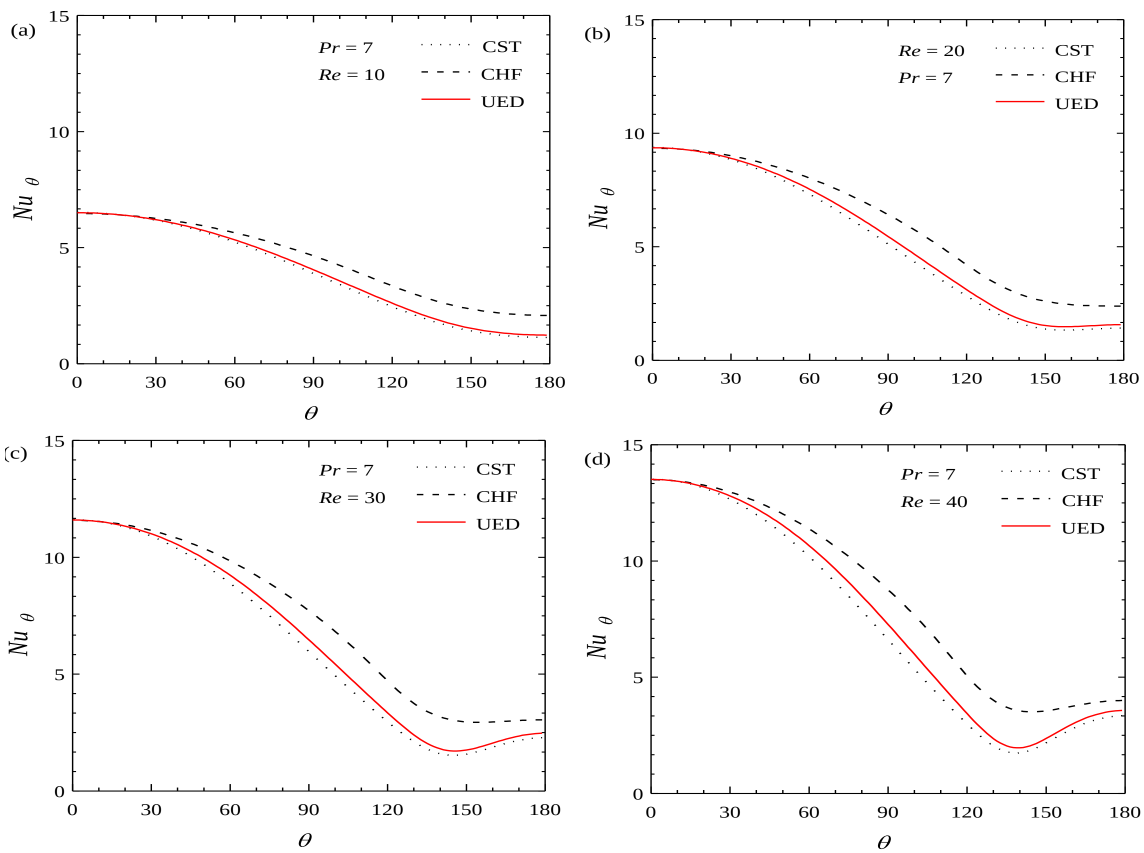

Fig- 8:Showing Nu_θ**for** ***Re*** **of 10 (a), 20 (b), 30 (c) and 40 (d) under CST, CHF and UED conditions**

The average Nusselt number Nuav was calculated by Eq.(13). Figure (9) shows the plot of Nu_{av} against Re. For three boundary conditions, the Nu_{av} was found to be proportional to $Re^{0.45}$ and as given in Eqs. (14) - (16), respectively. The Nu_{av} with uniform volumetric energy dissipation in the cylinder were about 11% lower than those with constant heat flux boundary condition and about 4% higher than those with constant surface temperature boundary condition.

For CST $\quad Nu_{av} = 1.346 \times Re^{0.45} \quad 10 \leq Re \leq 40 \quad (14)$

For CHF $\quad Nu_{av} = 1.511 \times Re^{0.46} \quad 10 \leq Re \leq 40 \quad (15)$

For UED $\quad Nu_{av} = 1.332 \times Re^{0.47} \quad 10 \leq Re \leq 40 \quad (16)$

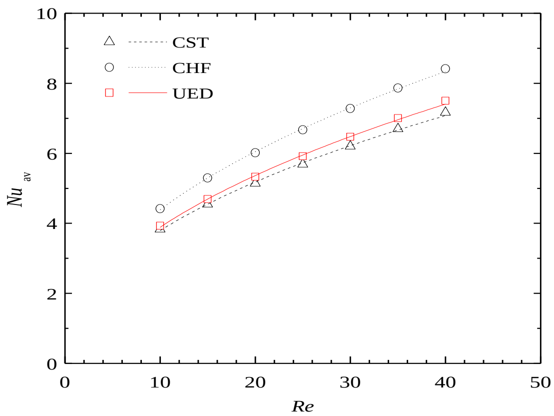

Fig-9:*Nu*$_{av}$under CST, CHF and UED conditions. *Pr* = 7

The results of present simulation were compared with the experimental data of (Park *et al.*,1998 and Hendersen 1995) (Tab 4). A maximum variation of 4% from the experimental data was found. Constant heat flux boundary was seen to yield the highest local and average Nusselt number values.

Conclusions: A two-dimensional numerical analysis was carried out using Fluent for heat transfer from a circular cylinder with uniform volumetric energy dissipation (conjugate boundary condition), constant surface temperature and constant heat flux under an unconfined space. The average Nusselt number with uniform volumetric energy dissipation in the cylinder were about 11% lower than those with constant heat flux boundary condition and about 4% higher than those with constant surface temperature boundary condition. The average Nusselt numbers for three boundary conditions are well represented by correlations which can be useful for design.

REFERENCES

Batchelor, G.K. An Introduction to Fluid Dynamics. 1st ed. Cambrige University Press, (2000).

Bharti, R. P., R. P. Chhabra, and V. Eswaran. A numerical study of the steady forced convection heat transfer from an unconfined circular cylinder. Heat Mass Transfer, 43(7): 639-648 (2007).

Eckert, E.R.G. andE. Soehngen. Distribution of heat transfer coefficients around circular cylinders in cross-flow at Reynolds number from 20 to 500. Trans. ASME, 51-F9: 343–347 (1953).

Gschneidner, K. A. and V. K. Pecharsky. Thirty years of near room temperature magnetic cooling: Where we are today and future prospects, Int. J. Refrigeration, 31: 945-961 (2008).

Hanafi, A. S., S. A. El-Sayed andM. E. Mostafa. Fluid flow and heat transfer around circular cylinder - flat and curved plates combinations. Exp. Thermal Fluid Sci., 25(8): 631-649 (2002).

Henderson, R. D. Details of the drag curve near the onset of vortex shedding. Physics Fluids, 7(9): 2102-2104 (1995).

Kitanovski, A. andP. W. Egolf. Innovative ideas for future research on magnetic technologies, Int. J. Refrigeration, 33(3): 449-464 (2010).

Nakamura, H. and T. Igarashi. Variation of Nusselt number with flow regimes behind a circular cylinder for Reynolds numbers from 70 to 30000. Int. J. Heat Mass Transfer, 47(23): 5169-5173 (2004).

Nielsen, K. K., C. R. H. Bahl, A. Smith, R. Bjork, N. Pryds and J. Hattel. Detailed numerical modeling of a linear parallel-plate Active Magnetic Regenerator. Int. J. Refrig., 32: 1478-1486 (2009).

Park, J., K. Kwon and H. Choi. Numerical solutions of flow past a circular cylinder at Reynolds numbers up to 160. KSME Int. J., 12(6): 1200-1205 (1998).

Versteeg, H. K., W. Malalasekera. An Itroduciton To Computational Fluid Dynamics : The Finite Volume Method. 2nd ed. Prentice Hall (2007).

Wang, M. Y. and J. G. Georgiadis. Conjugate forced convection in crossflow over a cylinder array with volumetric heating. Int. J. Heat Mass Transfer, 39(7): 1351-1361 (1996).

Williamson, C. H. K. Vortex dynamics in the cylinder wake. Ann. Review Fluid Mech. 28: 477-539 (1996).

Yoon, H. S., J. B. Lee, and H. H. Chun. A numerical study on the fluid flow and heat transfer around a circular cylinder near a moving wall. Int. J. Heat Mass Transfer. 50(17-18): 3507-3520 (2007).

Yu, B. F., M. Liu, P. W. Egolf and A. Kitanovski. A review of magnetic refrigerator and heat pump prototypes built before the year 2010, Int. J. Refrig., 33: 1029-1060 (2010).

Zukauskas, A., J. Ziugzda and G. F. Hewitt. Heat transfer of a cylinder in crossflow, Washington ; London: Hemisphere. 208p (1985).